Asian Journal of Chemistry; Vol. 38, No. 4 (2026), 949-955
ASIAN JOURNAL OF CHEMISTRY
https://doi.org/10.14233/ajchem.2026.35465

Development of Chalcone-Derived Polyurethane and Hybrid Composites with Superior Thermal and Corrosion Resistance Properties

POOVIZHI UMASANKAR, KRISHNAN LAKSHMANAN, T. SIVARAMAKRISHNAN and G. ELANGO*,

Department of Chemistry, Kalaignar Karunanithi Government Arts College, Tiruvannamalai-606601, India

*Corresponding author: E-mail: profelangoggactvm@gmail.com

Received: 16 December 2025 *Accepted*: 6 February 2026 *Published online*: 8 April 2026 AJC-22315

A chalcone-derived diol was synthesised and utilised for the production of polyurethane and its acrylic- and garnet-modified derivatives. The structural characteristics of the synthesised systems were elucidated *via* FT-IR and NMR studies, confirming the effective integration of urethane linkages, acrylic groups and garnet fillers. UV–Vis spectral study indicated π–π* and n–π* transitions in chalcone polyurethane, a bathochromic shift in acrylic polyurethane attributed to the extended conjugation and increased absorption in garnet polyurethane resulting from interfacial charge-transfer interactions. Thermal analyses (DSC, TGA and DTA) revealed that acrylic modification and garnet insertion enhanced crosslinking density, postponed degradation and elevated char yield, with garnet polyurethane displaying enhanced thermal resistance. Wettability study revealed a systematic transition from moderate hydrophilicity in chalcone polyurethane to increase the hydrophobicity in acrylic and garnet systems, due to surface alteration and filler-induced roughness. Electrochemical impedance spectroscopy validated the superior anticorrosive properties of garnet polyurethane, demonstrated by elevated charge transfer resistance and diminished ion diffusion. The findings collectively demonstrate that chalcone-derived polyurethanes, especially the garnet-reinforced composite, exhibit superior thermal stability, optical absorption, surface hydrophobicity and corrosion resistance, highlighting their potential as multifunctional protective coatings for advanced applications.

Keywords: Chalcone, Acrylic, Garnet, Corrosion resistance, Polyurethane.

INTRODUCTION

Polyurethane (PU) is a block copolymer composed of repeating structural units containing urethane linkages (–NH-CO-O-) and widely used due to its excellent mechanical strength, chemical resistance and structural versatility. These properties are arised due to its microphase-separated architecture of alternating soft and hard segments, which enable tunable flexibility and performance through molecular design [1,2]. Chalcone derived polyurethane is a type of polyurethane formed by integrating chalcone-based diols or polyols into its polymer backbone. The α,β-unsaturated carbonyl groups in chalcone provide rigidity, which boosts the thermal and mechanical performance of the polymer [3-5]. The aromatic nature of chalcone also enhances interfacial bonding, chemical resistance and electrochemical stability, making the material well-suited for applications such as protective coatings, corrosion-resistant layers and electroactive systems [6-8]. Moreover, the structure can be tailored through the choice of diisocyanate and chalcone derivative, allowing control over surface properties like hydrophobicity and ionic conductivity [9,10].

Polyurethane has been extensively investigated for its application as a protective coating on a wide range of substrates, including metals and wood [11-13]. Polyurethane coatings are applied using different methods, from traditional techniques like brushing and spraying to more advanced methods such as electrophoretic deposition [14,15]. Over time, these coatings can degrade, reducing the lifespan of both the coating and the material beneath it [16,17]. If cracks or defects form, moisture and oxygen can enter, leading to corrosion in metal surfaces [18,19].

In this study, a chalcone-based diol was successfully synthesized and subsequently employed in the preparation of poly-urethane systems, including acrylic-modified and garnet-reinforced composites. The structural characterization was confirmed using FT-IR and NMR analyses, while the thermal stability and corrosion resistance properties were systematically evaluated.

EXPERIMENTAL

Isophorone diisocyanate (IPDI) and dibutyltin dilaurate (DBTDL), used as cross-linker and catalyst, respectively, were purchased from Tokyo Chemical Industry Co., Ltd., Japan. Potassium hydroxide (Merck ≥ 99 %), 4-hydroxybenzaldehyde (reagent grade Aldrich, 90%), magnesium sulphate (Across 97%), acetone (analytical grade ≥ 99.9%) were used as received. Deionised water used throughout the study.

Characterisation: ^{1}H and ^{13}C NMR spectra were recorded on an Agilent NMR Systems VNMRS 400 spectrophotometer at 25 ºC in $CDCl_3$ or in DMSO-d_6, with $Si(CH_3)_4$ as an internal standard. ABB Bomem (Model MB3000) FT-IR spectrometer was used to record IR spectrum using KBr pellet method. Differential scanning calorimetry (DSC) was performed on Perkin-Elmer Diamond DSC from 10 to 400 ºC with a heating rate of 10 ºC min^{-1} under nitrogen flow. Thermal gravimetric analysis (TGA) was performed in Perkin Elmer Diamond TA/TGA with a heating rate of 2 ºC min^{-1} from 30 ºC under nitrogen flow, up to a maximum temperature of 700 ºC. Water absorption studies were done by contact angle meter (KYOWA, Dme - 210). Corrosion behaviour was studied by impedance analyser the samples were measured by precision LCR Meter (Agilent 4284 A).

Synthesis of chalcone based polyurethane: A 10 mL of acetone was taken into clean 100 mL two-necked round bottomed flask followed by the addition of 3 mL of ethanolic KOH solution dropwise while stirring at room temperature for 1 h. Then, 5 g of 4-hydroxybenzaldehyde was slowly added and the reaction mixture was refluxed for 12 h. A blood red colour turned into yellow colour. The reaction mixture was cooled to room temperature and finally poured into ice water the precipitate was filtered and dried. Yield: 80%.

In next step, 3 g of above prepared the olefine containing bisphenol product taken as a reactant was mixed with 3 mL of isophorone diisocyanate (IPDI) in a three-necked round bottomed flask, stirred and then refluxed with a suitable condenser and nitrogen inlet. Temperature was maintained at 80 ºC for 48 h and then added 2 drops of dibutyltin dilaurate (DBTDL) as a catalyst (**Scheme-I**). Upon completion of the reaction, the mixture became semi-viscous, after which it was cooled and further characterized.

Loading of PU with garnet filler: The synthetic chalcone based polyurethane was combined with garnet particles to obtain reinforced composite systems as an inorganic filler. The integration of garnet was executed *via* a magnetic stirring method to attain homogeneous distribution of the filler within the polymer matrix. A precise amount of garnet powder (2 g) was added to the PU resin while maintaining the constant mechanical agitation. The mixture was blended under controlled speed and time conditions to avoid particle agglomeration and achieve uniform garnet dispersion in the matrix.

RESULTS AND DISCUSSION

FTIR spectral studies: The structural validation of synthesised chalcone-based system was conducted with FT-IR spectroscopy. The spectrum of the acyclic chalcone-derived diol (Fig. 1a) displayed a large band about 3400 cm^{-1}, indicative of the stretching vibration of hydroxyl (–OH) groups, so affirming the existence of terminal diol functionalities. The C=O stretching vibration of the chalcone moiety was detected near 1650 cm^{-1}, whereas the aromatic C=C stretching occurred at 1600-1580 cm^{-1}, supporting the conjugated aromatic structure.

The spectrum of PU (Fig. 1b) shows the attenuation of the –OH stretching band and the appearance of a pronounced absorption band at 3330-3320 cm^{-1}, signifying the formation of urethane N–H groups. An intense absorption between 1725 and 1700 cm^{-1} was attributed to the carbonyl stretching of urethane links, hence validating the successful reaction between diol and diisocyanate. The band at 1240-1220 cm^{-1} corresponds to C–N stretching of the urethane group, whereas absorptions near 1540 cm^{-1} are attributed to N–H bending vibrations.

The spectrum of acrylic polyurethane (Fig. 1c) shows the distinctive urethane absorptions (N–H at ~3320 cm^{-1}, C=O at ~1715 cm^{-1} and C–N at ~1240 cm^{-1}), along with the presence of additional bands. The absorption bands observed at ~1640-1635 cm^{-1} were attributed to C=C stretching vibrations of the

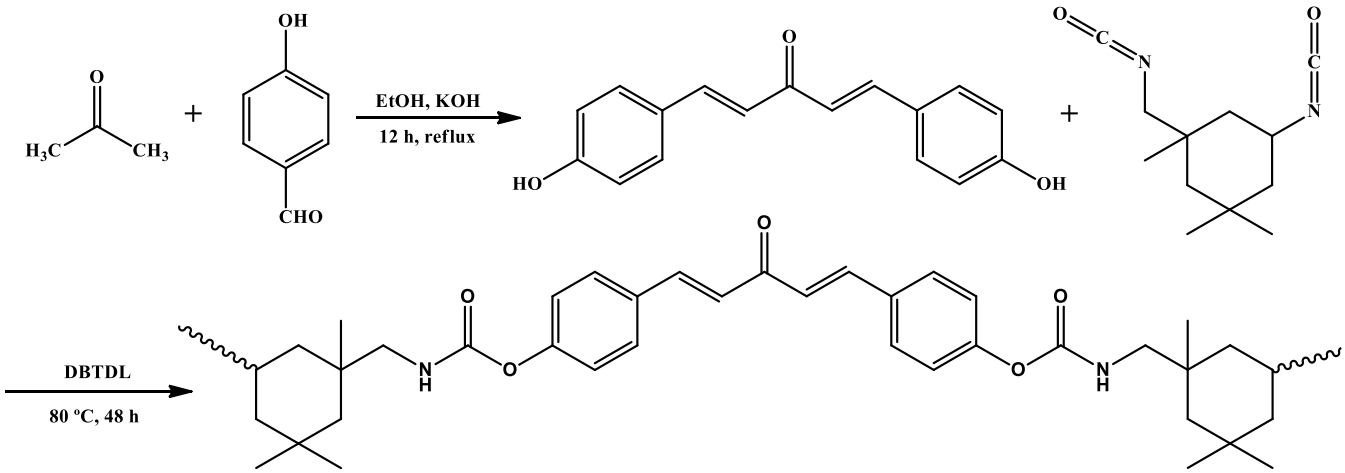

Scheme-I: Schematic diagram olefinic containing bisphenol based polyurethane

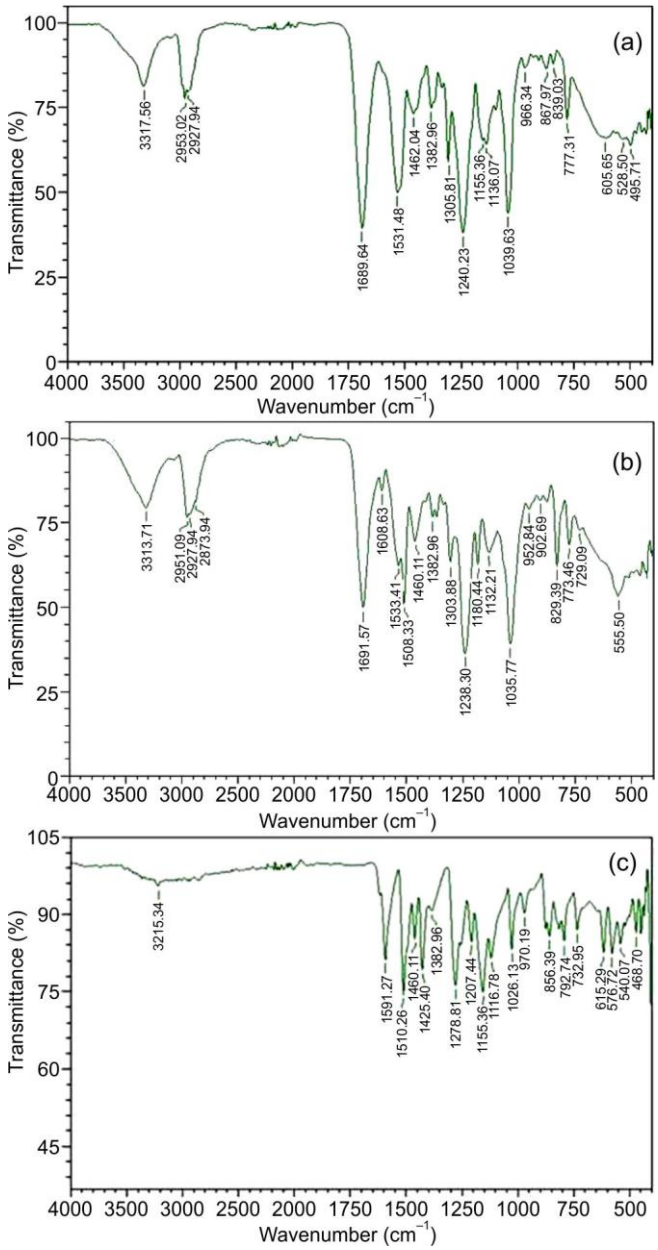

Fig. 1. FT-IR spectra of (a) acyclic chalcone based diol, (b) acyclic diol based polyurethane and (c) acyclic diol based acrylic polyurethane

acrylic groups, confirming successful incorporation of the acrylic functionality. The broadened bands in the 1100-1000 cm^{-1} region correspond to C–O–C stretching vibrations associated with the acrylic moiety.

In the garnet polyurethane spectrum (Fig. 2), identical urethane bands were detected (N–H ~3325 cm^{-1}, C=O ~1715 cm^{-1}, C–N ~1240 cm^{-1}). The other prominent absorptions between 670–560 cm^{-1} were observed, indicative of metal–oxygen (M–O) stretching vibrations, hence verifying the successful integration of garnet filler into the polyurethane matrix. The decrease in the C=O stretching frequency signifies intermolecular interactions between the polymer chains and garnet particles. Consequently, FT-IR spectral analysis unequivocally validated the sequential synthesis of diol, polyurethane, acrylic polyurethane and garnet polyurethane. The emergence of novel functional group absorptions and the

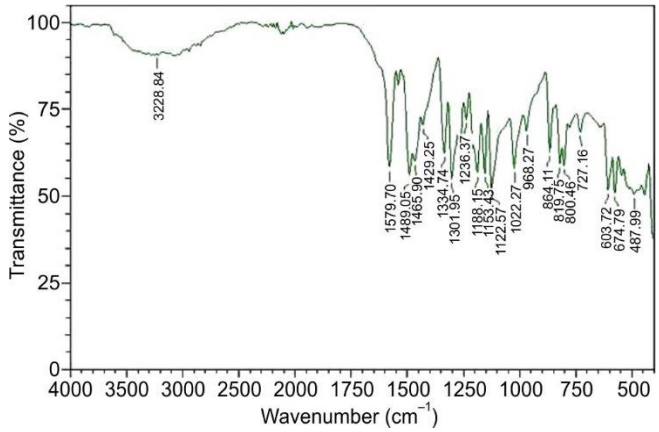

Fig. 2. FT-IR spectrum of acyclic diol based garnet polyurethane

alteration or elimination of original peaks serve as compelling evidence for the successful synthesis and modification of chalcone-based polymer systems.

NMR spectral studies: In the ^{1}H NMR spectrum (Fig. 3a) aliphatic proton signals were observed in the δ 1.0-2.3 ppm region. Hydroxyl protons appeared as a broad singlet at δ 5.5 ppm, confirming the diol formation. The ^{13}C NMR spectrum (Fig. 3b) displayed aliphatic carbon signals between δ 20-40 ppm, along with distinct peaks at δ 60-65 ppm corresponding to hydroxyl-bearing carbons. The absence of a carbonyl carbon signal confirmed successful reduction of the acyclic ketone to a diol compound.

Adsorption performance study: The optical absorption characteristics of the produced polymers were examined *via* UV-Vis spectroscopy. A unique absorption band for polyurethane (Fig. 4a) was identified in the 270-280 nm region, corresponding to π–π* transitions of the aromatic rings in the chalcone backbone. A diminished absorption band at around 320-330 nm can be ascribed to n–π* transitions of the urethane carbonyl moieties. These characteristics align with earlier findings on aromatic polyurethanes, wherein both π–π* and n–π* transitions predominate in the near-UV spectrum. The acrylic polyurethane (Fig. 4b) exhibited a minor bathochromic shift in absorption maxima (~285-295 nm) relative to pure polyurethane. The red shift results from prolonged conjugation and π-electron delocalisation caused by acrylic properties [20]. The comparable changes have been observed in acrylic-modified polyurethane systems, wherein the vinyl and ester groups augment conjugation and boost light absorption. The absorption spectrum of garnet polyurethane (Fig. 4c) displayed a notable red shift (~300-310 nm) and an enhancement in band intensity. The enhanced absorbance signifies robust interfacial contacts between the garnet nanoparticles and the polymer matrix. These interactions facilitate charge-transfer transitions and increased electronic delocalisation, a feature frequently observed in polymer–inorganic nanocomposites [21]. The inclusion of garnet generates localised states that enhance light-harvesting efficiency and expand the optical window, consistent with previous research on polyurethane oxide nanocomposites. The UV-Vis results substantiate the gradual alteration of chalcone-based polyurethane, with acrylic groups facilitating prolonged conjugation and garnet nanoparticles augmenting optical absorption *via* interfacial charge

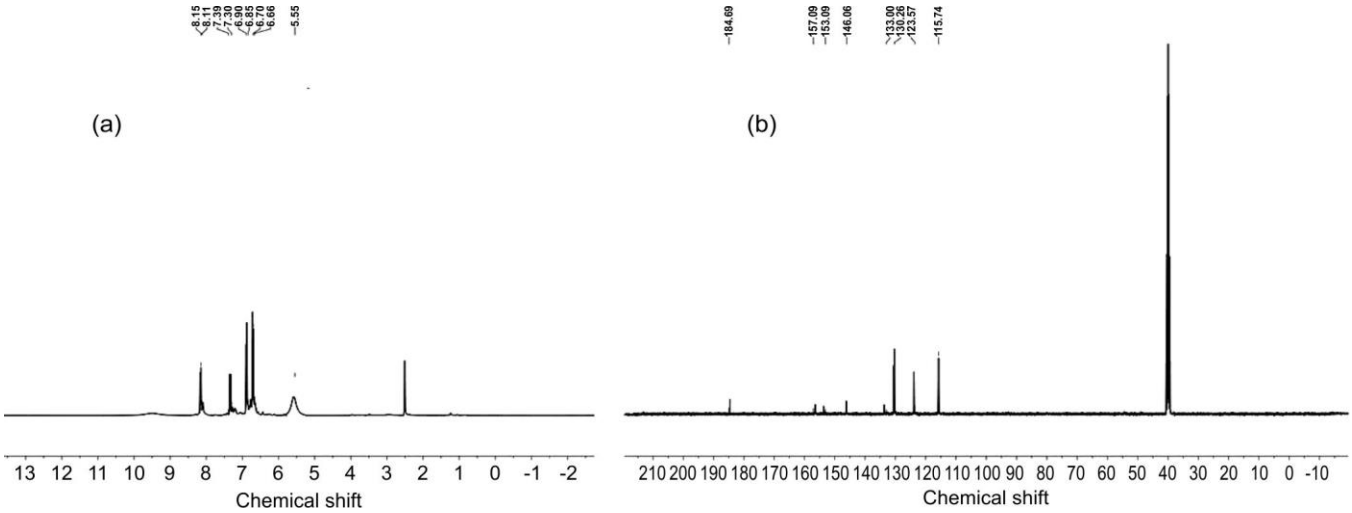

Fig. 3. (a) ^{1}H NMR and (b) ^{13}C NMR spectra of acyclicketone based diol compound (A)

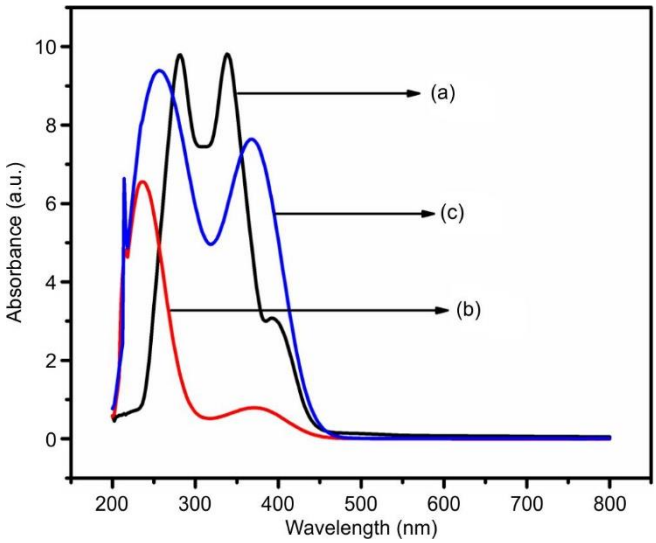

Fig. 4. UV-vis spectra of (a) acyclic chalcone containing diol based polyurethane, (b) acrylicpolyurethane and (c) garnet polyurethane

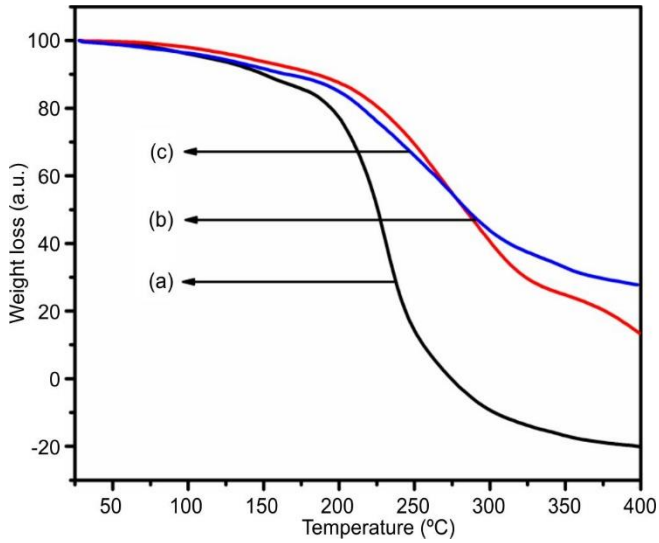

Fig. 5. TGA curves of (a) acyclic chalcone containing diol based polyurethane, (b) acrylic polyurethane and (c) garnet polyurethane

transfer. These results indicate possible uses in optoelectronic and ultraviolet-shielding materials.

Thermal stability studies: The thermal stability of the produced polyurethanes was assessed by thermogravimetric analysis (TGA). The acyclic chalcone diol-derived polyurethane (Fig. 5a) demonstrated a two-phase breakdown pattern. The initial weight loss, occurring between 250-320 ºC, is ascribed to the degradation of urethane links and soft segment chains. The second significant weight loss, occurring between 380-450 ºC, pertains to the decomposition of hard segment domains and the aromatic backbone. The char yield at 600 ºC was moderate, signifying restricted heat resistance. These findings align with previous studies on the degradation of segmented polyurethane [22]. The acrylic polyurethane (Fig. 5b) exhibited a somewhat elevated onset decomposition temperature (~270 ºC) in comparison to the diol-based polyurethane, indicating the stabilizing influence of acrylic functionalities. The higher heat stability is due to increased crosslinking density and conjugation from acrylic groups, which postpone the cleavage of urethane bonds. The ultimate degradation over 450 ºC yielded an increased char residue, indicating enhanced flame-retardant properties. The garnet polyurethane (Fig. 5c) had the greatest thermal stability among the three samples. The earliest disintegration happened around 290-310 ºC, but the primary degradation transpired above 400 ºC, suggesting that garnet nanoparticles function as a thermal barrier. The inclusion of inorganic filler limits chain mobility and reduces volatile emissions, therefore promoting char formation. At 600 ºC, the garnet polyurethane exhibited the maximum char production, affirming its exceptional resistance to heat breakdown. These results correspond with earlier research on polymer–inorganic nanocomposites indicating that metal oxide fillers enhance the thermal stability of polyurethane systems. The TGA results indicate that structural alteration and filler integration progressively improve the thermal stability of chalcone-based polyurethane, with garnet polyurethane demonstrating the most favourable stability for high-temperature applications.

Thermal studies: The acyclic chalcone diol-based polyurethane (Fig. 6a) demonstrated an endothermic transition

between 250-320 ºC, linked to the disintegration of urethane links and the deterioration of soft segments. A second significant endothermic peak was seen at 380-440 ºC, indicative of the decomposition of hard segment domains and the aromatic backbone. These transitions signify a two-step degrading mechanism characteristic of segmented polyurethane systems [23]. The thermal transition onset for acrylic polyurethane (Fig. 6b) migrated to elevated temperatures (~270-330 ºC), indicating enhanced thermal stability. This improvement results from heightened crosslinking density and conjugation provided by the acrylic moieties, which reinforce the polymer backbone and postpone bond cleavage. The second disintegration phase above 450 ºC yielded a greater char concentration than the diol-based polyurethane, indicating enhanced flame resistance.

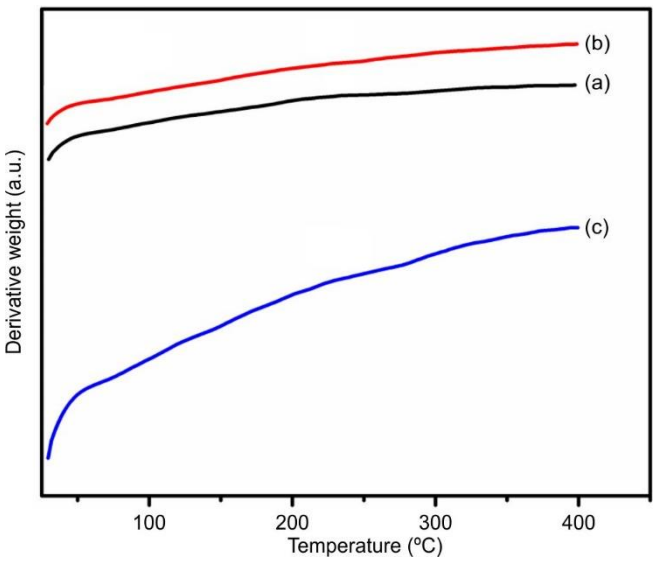

Fig. 6. DTA thermograms of (a) acyclic chalcone containing diol based polyurethane, (b) acrylic polyurethane and (c) garnet polyurethane

The garnet polyurethane (Fig. 6c) exhibited the greatest stability among the three systems. The preliminary endothermic reaction was observed around 290-340 ºC, but the major decomposition transpired beyond 420 ºC, signifying a notable change in thermal stability [24]. The integration of garnet nanoparticles serves as a barrier to thermal transfer and volatile emission, hence promoting char formation and diminishing the degradation rate. The expanded high-temperature endotherm suggests enhanced interfacial bonding between the inorganic filler and polymer matrix, in agreement with earlier reports on polyurethane-inorganic nanocomposites [25]. Thus, a progressive increase in thermal stability is observed, with garnet-reinforced polyurethane exhibiting the highest resistance to thermal degradation. This improvement can be attributed to the combined influence of structural modification and inorganic reinforcement.

Curing behaviour studies: The curing characteristics and thermal transitions of garnet polyurethane were examined *via* differential scanning calorimetry (DSC). The DSC thermogram exhibited an endothermic transition associated with the glass transition temperature (T_g) within the region of 55-65 ºC, indicative of the amorphous soft segment domains of polyurethane. A distinct T_g indicates the microphase separated architecture of hard and soft segments, as frequently documented in segmented polyurethane systems [26,27]. An exothermic peak detected at 180-200 ºC is indicative of the curing/rearrangement of residual isocyanate groups and chain extension processes. The addition of garnet particles affected the curing process by increasing crosslinking density, resulting in a little shift of the exothermic peak to elevated temperatures. This suggests that the filler functions as a reinforcing phase, limiting the mobility of polymer chains and thereby enhancing heat stability. A secondary transition was observed in the region of 250-260 ºC, linked to the melting or relaxation of ordered hard segment domains. This extent of transition indicates that garnet nanoparticles developed heterogeneity in the polyurethane matrix, aligning with the findings from polymer-inorganic nanocomposites [28]. The DSC study reveals that garnet addition promotes crosslinking and improves thermal stability by restricting chain mobility and increasing the energy required for segmental motion (Fig. 7). These results align with other studies indicating that inorganic fillers improved the curing behaviour and temperature transitions of polyurethane-based nanocomposites.

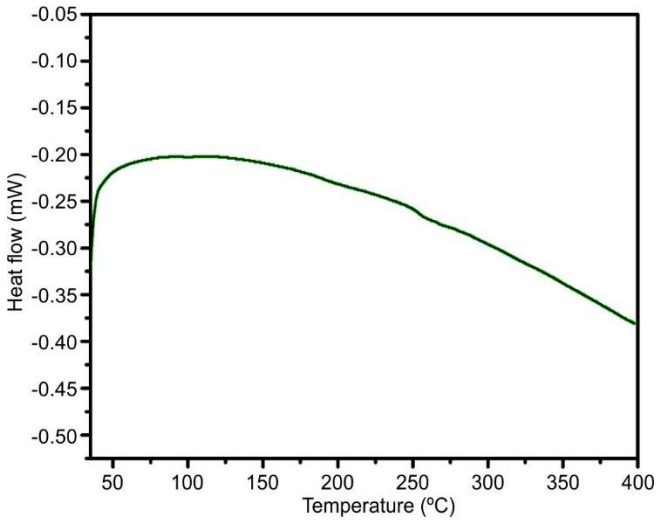

Fig. 7. DSC spectrum of garnet polyurethane

Wettability analysis: The wettability of the synthesised polyurethane systems was assessed by contact angle measurements. The acyclic chalcone-derived polyurethane (Fig. 8a) had a moderate contact angle, signifying a balance between hydrophilic urethane groups and hydrophobic aromatic components [29]. The surface energy was adequate to permit partial water spreading, aligning with typical polyurethane behaviour, wherein hydrogen bonding of urethane links affects wettability. The acrylic polyurethane (Fig. 8b) exhibited a greater contact angle than the chalcone-based polyurethane, indicating enhanced hydrophobicity. The incorporation of acrylic groups develops the supplementary non-polar domains, thereby diminishing surface energy and improving water repellency [30]. The garnet polyurethane (Fig. 8c) demonstrated the highest contact angle of the three systems, signifying a pronounced hydrophobic nature. The integration of garnet nanoparticles further enhanced surface roughness

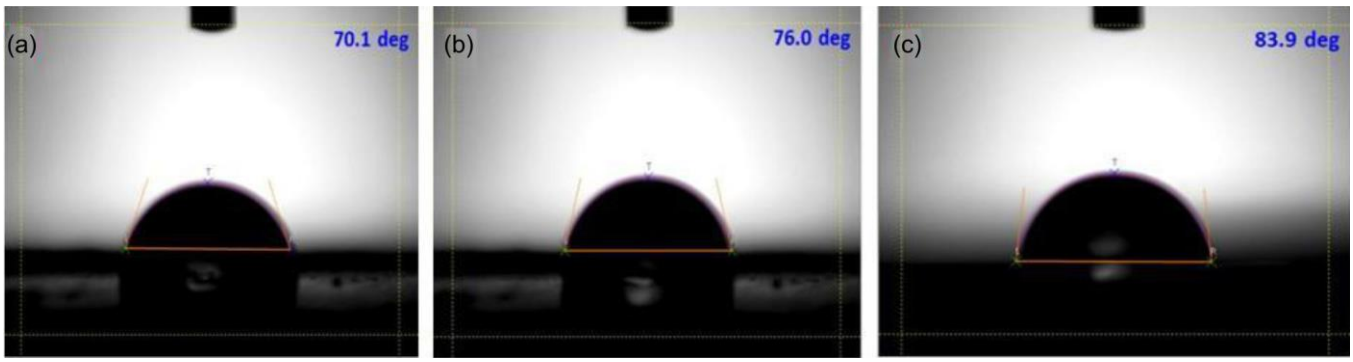

Fig. 8. Contact angle images of (a) chalcone polyurethane, (b) acrylic polyurethane and (c) garnet polyurethane

and diminished surface free energy by developing micro/nano-structures that inhibit wetting. This behaviour aligns with the Cassie-Baxter model of wettability, wherein the surface roughness and low-energy domains enlarge water repellency [31].

Electrochemical impedance analysis (EIS): The electrochemical impedance spectroscopy (EIS) was utilised to assess the anticorrosive efficacy of the acyclic chalcone diol-based garnet polyurethane. The spectrum (Fig. 9) displays a distinct semicircular arc, indicative of a charge transfer-controlled electrochemical process. The high-frequency intercept on the real axis represents the solution resistance (R_s), which is comparatively low, signifying excellent ionic conductivity of the electrolyte medium. The extensive diameter of the semicircle indicates the charge transfer resistance (R_{ct}), implying that the polymer coating offers a very resistant barrier at the electrode–electrolyte contact. The elevated R_{ct} value signifies that the coating efficiently inhibits the corrosion reaction by constraining electron transfer and limiting ion movement [32]. At lower frequencies, a minor diffusion-related tail is evident, attributable to Warburg-type impedance, indicating sluggish mass transport inside the polymer matrix [33]. The inhibition of this diffusion behaviour further substantiates the density and uniformity of the polyurethane coating, which impedes electrolyte infiltration into the underlying metal substrate. The findings indicate that integrating acyclic chalcone diol into the polyurethane backbone improves the corrosion resistance of the coating by enhancing interfacial stability and diminishing the surface's electrochemical activity.

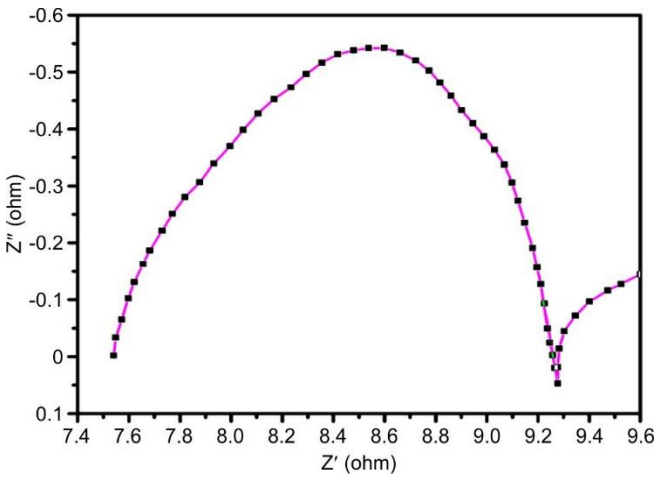

Fig. 9. Nyquist plot of the acyclic chalcone diol based garnet polyurethane

Conclusion

In this study, chalcone-based diol was successfully synthesised and subsequently utilised to prepare polyurethane hybrid composites including acrylic-modified and garnet-reinforced composites. The structural characterisation through FT-IR and NMR confirmed the successful formation of the chalcone-based based polymer backbones and their modifications. UV-Vis spectroscopy revealed enhanced optical absorption due to extended conjugation in acrylic polyurethane and interfacial charge-transfer interactions in garnet polyurethane. Thermal studies (DSC, TGA and DTA) demonstrated that the incorporation of acrylic groups and garnet nanoparticles significantly improved the thermal stability, crosslinking density and char yield of the polyurethane systems. Wettability analysis indicated a clear transition from moderate hydrophobicity in chalcone-based polyurethane to enhanced hydrophobicity in acrylic and garnet composites, attributed to chemical modifications and surface roughness introduced by garnet fillers. The electrochemical impedance spectroscopy further confirmed that the garnet polyurethane exhibited superior anticorrosive performance due to high charge transfer resistance and reduced ion diffusion across the coating. These findings highlight the potential of these novel polymer–inorganic hybrid materials as advanced protective coatings for applications requiring durability in harsh environments.

ACKNOWLEDGEMENTS

The authors thank Department of Chemistry, Kalaignar Karunanithi Government Arts College, Tiruvannamalai and the research facilities provided by Department of Chemistry, Anna University, Chennai, India to carry out the research work.

CONFLICT OF INTEREST

The authors declare that there is no conflict of interests regarding the publication of this article.

DECLARATION OF AI-ASSISTED TECHNOLOGIES

During the preparation of this manuscript, the authors used an AI-assisted tool(s) to improve the language. The authors reviewed and edited the content and take full responsibility for the published work.

REFERENCES

1. Y. Tian, Y. Wei, M. Wang, J. Wang, S. Li, X. Qin and L. Zhang, *Macromol. Rapid Commun.*, **47**, e00727 (2026); https://doi.org/10.1002/marc.202500727
2. Y. Luo, Q. Lu, J. Lu, Z. Chen, C. Li, Z. Luo, W. Cai, C.-H. Li, Z. Fei, Q. Lu and Y. Liu, *Mater. Horiz.*, **13**, 2438 (2026); https://doi.org/10.1039/D5MH01806D
3. T. Nawaz, A. Tajammal, A.W. Qurashi, M.-u. Nisa, D.N. Binjawhar and M. Iqbal, *Heliyon*, **10**, (2024); https://doi.org/10.1016/j.heliyon.2024.e30618
4. S. Takahashi, *J. Hematol. Oncol.*, **5**, 41 (2012); https://doi.org/10.1186/1756-8722-5-41
5. A.E. Russell and B.R. Gines, *Acc. Chem. Res.*, **56**, 1256 (2023); https://doi.org/10.1021/acs.accounts.2c00583
6. R.A. Menezes, C.N. Bhuvaneshwari, H. Venkatachalam and K.S. Bhat, *Discov. Appl. Sci.*, **7**, 814 (2025); https://doi.org/10.1007/s42452-025-07478-0
7. M.A. Fouda, A.M. Hassan, N.A. El-Shahat, H.M. El-Kemary and S.M. El-Sayed, *Electrochim. Acta*, **550**, 148117 (2026); https://doi.org/10.1016/j.electacta.2026.148117
8. S.R. Ratnaparkhi and C.U. Mahajan, *Corros. Sci.*, **207**, 110487 (2024); https://doi.org/10.1016/j.corsci.2024.110487
9. E.M. Sharshira, A.A. Ataalla, M. Hagar, M. Salah, M. Jaremko and N. Shehata, *Molecules*, **27**, 5409 (2022); https://doi.org/10.3390/molecules27175409
10. E. Negim, M. Shalash, K.M. Al Azzam, M.Z. Sagatbekovna, B.A. Kairatovna, A.T. Konstantinovich, N.A. Adlikhanovna, K.A. Ermekovna and B. Ravindran, *Int. J. Technol.*, **15**, 2009 (2024); https://doi.org/10.14716/ijtech.v15i6.7044
11. S. García, H. Fischer and S. Van Der Zwaag, *Prog. Org. Coat.*, **72**, 211 (2011); https://doi.org/10.1016/j.porgcoat.2011.06.016
12. G. Guedes, S. Wang, F. Fontana, P. Figueiredo, J. Lindén, A. Correia, R.J. Pinto, S. Hietala, F.L. Sousa and H.A. Santos, *Adv. Mater.*, **33**, 2007761 (2021); https://doi.org/10.1002/adma.202007761
13. S. Zafar, R. Kahraman and R. A. Shakoor, *Eur. Polym. J.*, **220**, 113421 (2024); https://doi.org/10.1016/j.eurpolymj.2024.113421
14. J. Jiang, H. Gao, M. Wang, L. Gao and G. Hu, *Polym. Eng. Sci.*, **63**, 3938 (2023); https://doi.org/10.1002/pen.26507
15. S. Ren, W. Zhou, K. Song, X. Gao, X. Zhang, H. Fang, X. Li and Y. Ding, *Prog. Org. Coat.*, **180**, 107571 (2023); https://doi.org/10.1016/j.porgcoat.2023.107571
16. X. He, Y. Zhang, J. He and F. Liu, *J. Coat. Technol. Res.*, **17**, 1255 (2020); https://doi.org/10.1007/s11998-020-00344-1
17. W. Zhang, N. Jiang, T. Zhang and T. Zhang, *J. Elastomers Plast.*, **53**, 296 (2021); https://doi.org/10.1177/0095244320933988
18. S. Jung, H.G. Jang, J.Y. Jo, Y.S. Kim, D.C. Lee and J. Kim, *ACS Appl. Mater. Interfaces*, **15**, 26028 (2023); https://doi.org/10.1021/acsami.3c04194
19. O. Bayer, *Angew. Chem.*, **59**, 257 (1947); https://doi.org/10.1002/ange.19470590901
20. Y. Shen, J. Liu, Z. Li, J. Luo, S. Wang, J. Tang, P. Wang, D. Wang, X. Wang, X. Hu and F. Zhang, *Int. J. Adhes. Adhes.*, **129**, 103583 (2024); https://doi.org/10.1016/j.ijadhadh.2023.103583
21. T. Zhang, Z. Liu, Y. Lu, Y. Wang, L. Zhu, S. Zhang, C. Wang, W. Chen, J. Zhang, G. Bai and W. Zhang, *Polymer*, **336**, 128879 (2025); https://doi.org/10.1016/j.polymer.2025.128879
22. R. Kubota and M. Shibata, *Polym. Bull.*, **82**, 2329 (2025); https://doi.org/10.1007/s00289-024-05620-3
23. J. Chen, Y. Zhu, X. Chang, D. Pan, G. Song, Z. Guo and N. Naik, *Adv. Funct. Mater.*, **31**, 2104686 (2021); https://doi.org/10.1002/adfm.202104686
24. S. Zafar, R. Kahraman and R. Shakoor, *Colloids Surf. A Physicochem. Eng. Asp.*, **703**, 135434 (2024); https://doi.org/10.1016/j.colsurfa.2024.135434
25. S. Naheed, Z. Siddique, A. Anjum, M. Salman, N. Rasool, A. Hassan, M. A. Bajaber, K. Jilani, M. Shahid and T. Khalid, *Discov. Mater.*, **5**, 232 (2025); https://doi.org/10.1007/s43939-025-00430-4
26. C. Hepburn, Polyurethane Elastomers, Springer Science & Business Media (2012).
27. M. Szycher, Structure–Property Relations in Polyurethanes, Szycher's Handbook of Polyurethanes, pp 37-86 (2012).
28. S.K. Srivastava and Y.K. Mishra, *Nanomaterials*, **8**, 945 (2018); https://doi.org/10.3390/nano8110945
29. J. Zhao, Z. Zhao, A. Hou, Q. Jiang, J. Xie, Q. Feng, Z. Li, Y. Li, G. Huang, J. Yan and X. Wang, *ACS Appl. Nano Mater.*, **7**, 28767 (2024); https://doi.org/10.1021/acsanm.4c06100
30. Y. Shiraki, *J. Appl. Polym. Sci.*, **141**, e55010 (2024); https://doi.org/10.1002/app.55010
31. Z. Rajabimashhadi, R. Naghizadeh, A. Zolriasatein, S. Bagheri, C. Mele and C.E. Corcione, *Polymers*, **15**, 1916 (2023); https://doi.org/10.3390/polym15081916
32. H. Yu, Z. Xu, T. Fang, M. Zhang, Y. Xu, J. Liu and X. Tan, *Polym. Adv. Technol.*, **35**, e6307 (2024); https://doi.org/10.1002/pat.6307
33. F. Lu, B. Song, P. He, Z. Wang and J. Wang, *RSC Adv.*, **7**, 13742 (2017); https://doi.org/10.1039/C6RA26341K